Reactive Power-Voltage-Based Voltage Instability Sensitivity Indices for Power Grid With Increasing Renewable Energy Penetration

BUKOLA BABATUNDE ADETOKUN[ID][1], **(Graduate Student Member, IEEE),**
JOSEPH OLORUNFEMI OJO[ID][2,3], **(Fellow, IEEE), AND**
CHRISTOPHER MAINA MURIITHI[4], **(Member, IEEE)**

[1]Department of Electrical Engineering, Pan African University Institute for Basic Sciences, Technology and Innovation, Jomo Kenyatta University of Agriculture and Technology, Nairobi, Kenya
[2]Department of Electrical and Computer Engineering, Tennessee Technological University, Cookeville, TN 38505, USA
[3]Department of Electrical Power Engineering, Durban University of Technology, Durban 4000, South Africa
[4]Department of Electrical Engineering, Murang'a University of Technology, Murang'a, Kenya

Corresponding author: Bukola Babatunde Adetokun (jesutunde@gmail.com)

ABSTRACT In this work, a reactive power-voltage (QV)-based framework to evaluate the voltage instability sensitivities of power system buses to increase in renewable energy (RE) penetration has been developed using two sensitivity indices, namely, Critical Voltage Sensitivity Index (CVSI) and Critical Reactive Power Sensitivity Index (CQSI). The rise or fall in the critical voltage level is measured by CVSI and the reactive power loss intolerance of each bus is evaluated by the CQSI as the RE penetration level increases. The bus sensitivity analysis obtained from the CVSI and CQSI provides information on the voltage instability sensitivity of each power system bus to increase in RE penetration level. The proposed methodology has been evaluated using IEEE 14-bus system and New England 39-bus system. DIgSILENT PowerFactory was used to perform the simulations and Matrix Laboratory (MATLAB) used to analyse the results. The sensitivity analysis of the buses can provide insights on the most suitable placement for large reactive loads or devices such as Flexible Alternating Current Transmission Systems (FACTS) as the RE penetration level (PL) increases.

INDEX TERMS DFIG-based wind energy conversion system, QV curve analysis, reactive power loss intolerance, renewable energy integration, solar photovoltaic system, voltage instability sensitivity indices.

I. INTRODUCTION

Renewable energy (RE) systems are rapidly being developed and employed as viable alternatives for the traditional fossil-fuel based generation systems [1]. This has particularly been necessitated as part of the global efforts towards mitigation of climate change effects. The need to meet the rising global energy demand has also informed intensified efforts toward renewable and sustainable energy investments world-wide. Wind Energy Conversion Systems (WECS) and Large-scale Solar Photovoltaic (SPV) systems are the leading renewable energy generation systems [2].

Meanwhile, the subject of 100% renewable energy grid as attracted much attention in recent times [3]–[6]. The

The associate editor coordinating the review of this manuscript and approving it for publication was Arash Asrari[ID].

authors in [3] presented a burden of proofs doubting the feasibility of 100% renewable-electricity systems, considering the enormous technical and economic constraints associated with it. However, the authors in [4] have presented convincing arguments in response to the evidence provided in [3], indicating that renewable penetration of 100% is achievable. The supportive evidence to this possibility is that some nations have already achieved significantly very high renewable generation. For instance, Iceland, Paraguay, Norway, Uruguay, Costa Rica, Brazil and Canada have attained 100%, 99%, 97%, 95%, 93%, 76% and 62% RE penetration respectively [6].

One of the major constraints for increasing renewable energy integration into the power grid is voltage stability [7], [8]. Voltage stability can limit the extent of renewable energy integration in power systems [9].

Therefore, this paper has explored scenarios of increasing RE penetration level (PL) up to 100% and the attendant voltage instability sensitivities of this increase in RE PL within the power system using Critical Voltage Sensitivity Index (CVSI) and Critical Reactive Power Sensitivity Index (CQSI). The CVSI evaluates the impact of increasing RE penetration on the rise in critical voltage level of the power system buses and the CQSI measures the reactive power loss intolerance of each bus within the power system.

Finding the critical bus in a power system is important because it gives insight on which area of the system is weakest and most prone to voltage instability. In addition, identifying the critical buses will enable the system operator to determine the appropriate location for additional voltage support or reactive power compensation in order to ensure continued stability of the system [10]–[12]. Different voltage stability indices have been developed by several authors [13]–[22]. A Simplified Voltage Stability Index (SVSI) has been proposed in [15]. The index utilizes voltage phasor measurements and topology of power system to estimate the voltage stability margin. Voltage collapse occurs when the SVSI value reaches 1 in a bus. In [21], Voltage Stability Index (VSI) based on power flow equations has been developed. This VSI has been formulated using the magnitudes of bus voltage and current in order to calculate the distance between the current operating point and point of voltage collapse. At no load condition, VSI value is 1, and at the point of voltage collapse, its value is 0. Moreover, the authors in [22] proposed a Voltage Collapse Prediction Index (VCPI) to predict voltage collapse in a power system. The VCPI formulation is based on system variables such as the bus voltage angle, voltage magnitude and admittance matrix of the system. The VCPI value varies from 0 to 1. Buses with VCPI value near zero indicates stable bus voltage. Detailed reviews of various voltage stability indices have been presented in [23], [24]

Furthermore, various studies have been carried out to assess the impact of renewable energy integration on power system stability [25]–[35]. Studies concerning the impact of wind energy integration on system stability are carried out in [28], [30], [31]. In particular, the authors in [31] evaluated the impact of integrating variable speed wind farms on the transient stability of power system using a sensitivity index based on the terminal voltage of the connected variable speed wind generator.

Moreover, the effect of utility-scale grid-tied solar PV system on voltage stability was investigated in [33]. The results of the investigation indicate that high solar PV penetration can enhance the bus voltage profiles, thereby reducing system instability. In [34], the analysis relating to the prospect of employing optimally-sized and optimally-dispatched solar PV with battery energy storage to improve voltage stability and minimize energy loss was also carried out.

None of the studies above considered scenarios of increasing RE penetration with the associated voltage instability sensitivities of the power grid buses. In addition, the bus sensitivity analysis carried out in this work is not limited to load buses only, but includes all buses except the slack bus. This gives a better insight on the overall voltage instability sensitivity of the power system buses with increase in RE penetration level (PL). Practical considerations such as the reactive power limits and the reactive power capability of the conventional generators and the RE conversion systems have been taken into account in this study. Both Doubly-Fed Induction Generator (DFIG)-based WECS and Large-scale solar photovoltaic (SPV) system have been considered in this work. In this study, the effect of increased renewable energy PL on the reactive power capability of power system buses has been evaluated using the Critical Reactive Power Sensitivity Index (CQSI). Moreover, the effect of increased RE PL on the critical voltage profile of the power system buses has been evaluated using Critical Voltage Sensitivity Index (CVSI). These indices have been developed using QV curve analysis. Renewable energy PL has been defined in this study as the proportion of the real power dispatched from renewable energy conversion systems (DFIG-based WECS and Solar PV system) to the overall real power dispatched from all generators within the system. Similar definition was adopted in [36].

The main contributions of this paper can be summarised as follows:

- The concept of QV curve analysis has been explored to develop two voltage instability sensitivity indices, namely CVSI and CQSI.
- These indices have been used to evaluate the sensitivity of each power system bus to increase in renewable energy penetration. The rise or fall in the critical voltage level is measured by CVSI and the reactive power loss intolerance of each bus is evaluated by the CQSI as the RE penetration level increases.
- The bus sensitivity analysis obtained from the CVSI and CQSI provides information on the voltage instability sensitivity of each power system bus to increase in RE PL. This can give insights on the appropriate location of large inductive loads or reactive power compensation devices as the RE penetration level increases.
- As an illustration of the application of these indices, IEEE 14-bus test system and IEEE 39-bus New England system, modelled in DIgSILENT PowerFactory, have been used as case studies. Different scenarios of RE mix and locations have been considered.

The rest of the paper is arranged as follows: Section II presents the modelling of DFIG-based WECS and solar PV system. Section III provides an overview of QV analysis and the development of the proposed sensitivity indices. The application of the proposed indices is presented and discussed in Section IV and V. Conclusion is provided in Section VI.

II. MODELLING OF RENEWABLE ENERGY CONVERSION SYSTEMS

This section presents the modelling of the DFIG-based WECS and solar PV system, which are considered in this work.

A. DFIG-BASED WECS MODELLING

The generic model of wind turbine and DFIG are provided in this subsection. The mechanical output power of a wind turbine can be expressed as [37]:

$$P_t = 0.5 C_p (\lambda, \beta) \rho A V_w^3 \tag{1}$$

where C_p is the coefficient of performance, which is the aerodynamic efficiency of the turbine. The λ and β are the tip speed ratio and pitch angle of the turbine blade respectively, ρ is the air density in kg/m^3, A is the area of turbine swept in m^2 and V_w is the wind speed in m/s.

The coefficient of performance indicates the proportion of the wind's kinetic energy converted to mechanical energy and can be expressed in terms of tip speed ratio (λ) and blade pitch angle (β) as [38]:

$$C_p (\lambda, \beta) = 0.5176 \left(\frac{116}{\lambda_1} - 0.4\beta - 5 \right) e^{\frac{-21}{\lambda_1}} + 0.0068\lambda \tag{2}$$

where

$$\frac{1}{\lambda_1} = \frac{1}{\lambda + 0.08\beta} - \frac{0.035}{\beta^3 + 1} \tag{3}$$

The tip speed ratio, λ is expressed as:

$$\lambda = \omega_t R_t / V_w \tag{4}$$

where ω_t is the rotor blade tip speed in rad/s, and R_t is the radius of the turbine blade.

The synchronously rotating reference frame model of DFIG is expressed as:

$$
\begin{aligned}
v_{qs} &= -r_s i_{qs} + \omega_e \lambda_{ds} + p\lambda_{qs} \\
v_{ds} &= -r_s i_{ds} - \omega_e \lambda_{qs} + p\lambda_{ds} \\
v'_{qr} &= -r_r i'_{qr} + (\omega_e - \omega_r) \lambda'_{dr} + p\lambda'_{qr} \\
v'_{dr} &= -r_r i'_{dr} - (\omega_e - \omega_r) \lambda'_{qr} + p\lambda'_{dr}
\end{aligned}
\tag{5}
$$

The flux linkage equations can be expressed as:

$$
\begin{aligned}
\lambda_{qs} &= - \left[L_{ls} i_{qs} + L_M \left(i_{qs} + i'_{qr} \right) \right] \\
\lambda_{ds} &= - \left[L_{ls} i_{ds} + L_M \left(i_{ds} + i'_{dr} \right) \right] \\
\lambda'_{qr} &= - \left[L'_{lr} i'_{qr} + L_M \left(i_{qs} + i'_{qr} \right) \right] \\
\lambda'_{dr} &= - \left[L'_{lr} i'_{dr} + L_M \left(i_{ds} + i'_{dr} \right) \right]
\end{aligned}
\tag{6}
$$

The active and reactive power expression for the stator (P_s, Q_s) and rotor (P_r, Q_r) circuits is given as [39]:

$$
\begin{aligned}
P_s &= 1.5 \left(v_{ds} i_{ds} + v_{qs} i_{qs} \right) \\
Q_s &= 1.5 \left(v_{qs} i_{ds} - v_{ds} i_{qs} \right) \\
P_r &= 1.5 \left(v'_{dr} i_{dr} + v'_{qr} i'_{qr} \right) \\
Q_r &= 1.5 \left(v'_{qr} i'_{dr} - v'_{dr} i'_{qr} \right)
\end{aligned}
\tag{7}
$$

where v_{qs} (v_{ds}) is the q-axis (d-axis) stator voltage, v'_{qr} (v'_{dr}) is the q-axis (d-axis) rotor voltage, i_{qs} (i_{ds}) is the q-axis (d-axis) stator current, i'_{qr} (i'_{dr}) is the q-axis (d-axis) rotor current, λ'_{qr} (λ'_{dr}) is the q-axis (d-axis) rotor flux linkage, r_s (r'_r) is the stator (rotor) resistance, L_{ls} (L'_{lr}) is the stator (rotor)
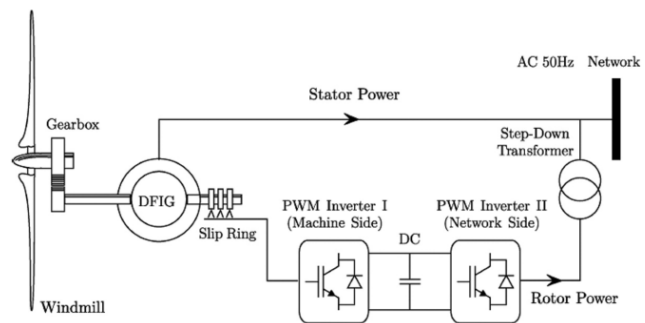

FIGURE 1. Schematic diagram of grid-connected DFIG-based WECS [41].

leakage inductance, L_M is the magnetising inductance, ω_e is the synchronous speed, ω_r is the rotor speed and p is the differential operator.

The DFIG is coupled to the wind turbine by a mechanical shaft, and the complete DFIG-WECS is connected to the power grid via both the stator and the rotor. The stator windings of the DFIG are directly connected to the grid but the rotor windings are fed through a back-to-back power electronic converter [40], [41]. The converter comprises the machine side converter and the grid side converter. The machine side converter controls the rotor speed and the reactive power while the grid side converter maintains the dc-link capacitor voltage at a constant level [42]. The schematic diagram of the grid-connected DFIG-based WECS is depicted in Fig. 1.

B. SOLAR PV SYSTEM MODEL

Solar PV array is formed by large numbers of solar cells grouped together in series and parallel. The single diode equivalent circuit of a solar cell is shown in Fig. 2a. Fig. 2b shows the corresponding circuit for a PV array made up of Ns series and Np parallel PV cells. The photocurrent produced by the solar cell is denoted as I_{ph}. I_D represents the forward current of the diode, D the cell photocurrent and I_{sh} is the current drawn by the shunt resistor. R_{se} and R_{sh} and are the intrinsic series and shunt resistances of the cell respectively and they account for the resistive losses of the cell.

The output current, I_{out} of a solar cell can be derived from the Kirchoff's Current Law applied to the circuit of Fig. 2a.

$$I_{out} = I_{ph} - I_o \left[\exp \left(\frac{q (V_{out} + I_{out} R_{se})}{nkT} \right) - 1 \right] - \frac{(V_{out} + I_{out} R_{se})}{R_{sh}} \tag{8}$$

For a PV array with Ns series and Np parallel cells, the output current, I_{out} is expressed as:

$$
\begin{aligned}
I_{out} = N_P I_{ph} &- N_P I_o \left[\exp \left(\frac{q}{nkT} \cdot \frac{N_P V_{out} + N_S R_{se} I_{out}}{N_P N_S} \right) - 1 \right] \\
&- \frac{N_P V_{out} + N_S R_{se} I_{out}}{N_S R_{sh}}
\end{aligned}
\tag{9}
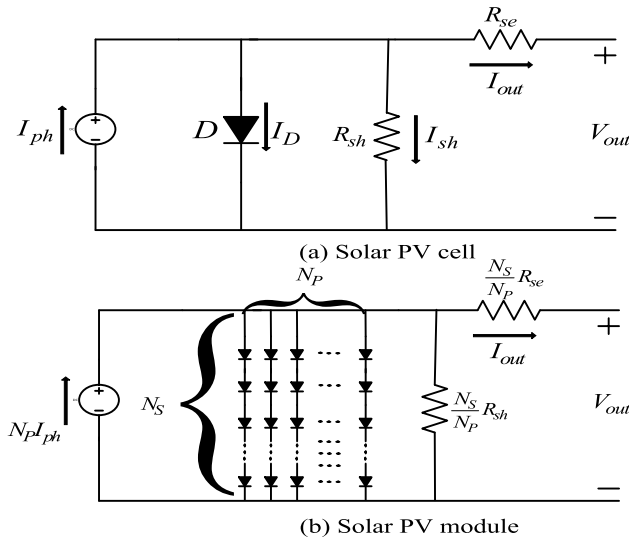$$

(a) Solar PV cell

(b) Solar PV module

FIGURE 2. Equivalent circuit of a solar PV cell and PV module.

where V_{out} is the output voltage of the solar PV cell, q is the electron charge, n is the ideality factor of the diode, k is the Boltzmann's constant and T is the operating temperature.

The dark saturation current, I_o is temperature-dependent and can be expressed as:

$$I_o = I_R \left[\frac{T}{T_R} \right]^3 \exp \left[\frac{qE_G}{nk} \left(\frac{1}{T} - \frac{1}{T_R} \right) \right] \quad (10)$$

where T_R is the reference temperature of 25°C (298.15K) at Standard Test Conditions (STC), I_R is the solar cell reverse saturation current at STC, and E_G is the bandgap energy of the solar cell semiconductor. The remaining four parameters, I_{ph}, n, R_{se}, and R_{sh} in Equation (9) also depends on the operating temperature and incident solar radiation [43].

The models of DFIG-based WECS and large-scale solar PV system in DIgSILENT PowerFactory has been used in this work. DIgSILENT PowerFactory is a well-known and proven simulation software for both industrial and academic purposes and the models are accurate for practical applications.

III. DEVELOPMENT OF THE QV-BASED SENSITIVITY INDICES: CVSI AND CQSI

This section provides a fundamental overview of QV curve analysis and the development of the proposed indices.

The QV curve indicates the variation and sensitivity of a bus voltage with respect to the injected/absorbed reactive power at that bus. The minimum point of the curve, where $dQ/dV = 0$, is the critical point (V_C, Q_C) of voltage stability for any specified bus. The critical voltage V_C, is the minimum voltage below which voltage instability will occur while the critical reactive power Q_C, is the minimum amount of reactive power required to maintain this voltage for the stable operation of the grid. If Q_C is negative, it implies that to maintain the stable operation of the grid, this critical amount of reactive power Q_C must not be lost or absorbed at the

specified bus so that the bus voltage does not fall below V_C. If Q_C is positive, then this value is the minimum amount of reactive power required to be injected at the bus in order to restore the power system from voltage collapse. This critical amount of reactive power is also known as the reactive power margin at the specified bus.

The two sensitivity indices, CVSI and CQSI are derived from the QV curve analysis for an N-bus system. The CVSI, denoted as V_{CSI}, and the CQSI, denoted as Q_{CSI} can be derived as follows:

Increase the renewable energy PL in steps from 0 to maximum PL. Set PL counter $i = 1 : L$ and bus counter $j = 2 : N$, where L is the number of penetration levels being considered and N is the total number of buses.

For each PL, obtain the corresponding percentage variation in critical voltage level for each bus, which is:

$$V_{CSI}(i,j) = \left[\left(V_{C(i,j)} - V_{C(1,j)} \right) / \left| V_{C(1,j)} \right| \right] \times 100\% \quad (11)$$

where $V_{C(1,j)}$ is the critical voltage at base case (0% PL) for bus j and $V_{C(i,j)}$ is the critical voltage at the ith PL for bus j.

Obtain the corresponding variation in reactive power for each bus, which is:

$$Q_{CSI}(i,j) = \left[\left(Q_{C(i,j)} - Q_{C(1,j)} \right) / \left| Q_{C(1,j)} \right| \right] \times 100\% \quad (12)$$

where $Q_{C(1,j)}$ is the critical reactive power at base case (0% PL) for bus j and $Q_{C(i,j)}$ is the critical reactive power at i^{th} PL for bus j.

V_{CSI} and Q_{CSI} at each PL are respectively, the percentage variations in critical voltage and critical reactive power from the base case values (0% PL). The bus with the most negative V_{CSI} is identified as the bus with the highest fall in critical voltage level and thus the least affected bus. On the other hand, the bus with the most positive V_{CSI} is the bus with the highest rise in critical voltage level as the renewable energy PL increases. A V_{CSI} value of zero at any bus(es) signifies that there is no variation in the critical voltages at such buses. Furthermore, the bus with the most negative Q_{CSI} is identified as the bus that is most tolerant to loss of reactive power as the penetration level (PL) of RE increases. However, the bus with the most positive Q_{CSI} value is the bus, which is most intolerant to loss of reactive power as the PL increases.

The voltage instability criterion is thus established as follows:

If the Q_{CSI} value of any bus becomes greater than or equal to 100% ($Q_{CSI} \geq 100\%$) at any penetration level, then the system has reached a condition of voltage collapse at that RE penetration level.

These indices measure the voltage instability sensitivities of each bus to increase in RE penetration level. The analysis thus provides insights on the most optimal location of large inductive loads or reactive power compensation devices in order to prevent voltage collapse of the system as the RE PL increases significantly.

Equations (11) and (12), which defines the proposed indices and the established voltage instability criterion are newly derived in this paper.

TABLE 1. Ranking of IEEE 14-bus system load buses: Comparison of CQSI with L-index and BPF.

Rank	Bus	RPM	Bus	L-index	Bus	BPF
1	Bus 14	68.19	Bus 14	0.222	Bus 14	0.122
2	Bus 12	70.52	Bus 12	0.194	Bus 12	0.118
3	Bus 13	83.21	Bus 13	0.138	Bus 13	0.114
4	Bus 11	84.13	Bus 11	0.099	Bus 11	0.112
5	Bus 10	89.52	Bus 10	0.079	Bus 10	0.108
6	Bus 9	100.46	Bus 9	0.066	Bus 9	0.098
7	Bus 7	115.66	Bus 7	0.049	Bus 7	0.078
8	Bus 4	222.23	Bus 4	0.037	Bus 4	0.024
9	Bus 5	232.43	Bus 5	0.031	Bus 5	0.020

A basic validation of the accuracy of these QV-based derived indices has been made by comparing the CQSI ranking at base case PL, which is essentially the reactive power margin (RPM) obtained from QV analysis with L-index [44] and bus participation factor (BPF) of the minimum eigenvalue [45]. Table 1 depicts the ranking comparison of the IEEE 14-bus system load buses from the least voltage-stable (weakest) to the most voltage-stable (strongest) bus.

The performance of the developed indices are evaluated with two power systems, namely, the IEEE 14-bus system and the IEEE 39-bus New England system. The next section therefore discusses the impact of increase in renewable energy penetration levels on the voltage instability sensitivities of each bus of the power system using CVSI and CQSI.

## IV. IEEE 14-BUS TEST SYSTEM CASE STUDY

Four different cases of RE integration are investigated for the IEEE 14-bus system. In the first case, only DFIG-based WECS is considered and is located at bus 14, which is the weakest bus. In the second case, DFIG-based WECS is located at bus 14 and solar PV at bus 12. In the third case, only DFIG-based WECS is considered and is located at bus 2, with the synchronous generator at bus 2 removed. In the fourth case, DFIG-based WECS is located at bus 2 and solar PV at bus 5. The single line diagram of the IEEE 14-bus test system is depicted in Fig. 3 and the system data are detailed in [46].

A. CASE 1: DFIG-WECS ONLY LOCATED AT BUS 14
In this case, only DFIG-based WECS is located at bus 14. The PL is increased in steps of 50MW from 0MW (0%) PL to 350MW (95.27%) PL. The bar chart of critical voltage sensitivity index is displayed in Fig. 4a and 4b. Fig. 4a shows the V_{CSI} plot with respect to the percentage PL while Fig. 4b depicts V_{CSI} with respect to the bus numbers. Both charts in the figure show that as far as the critical voltage level is concerned, bus 2 is negatively sensitive at all penetration levels while buses 4, 5, 9, and 14 are positively sensitive at all penetration levels, with bus 14 having the overall highest positive V_{CSI} value. Buses 3, 6, 7 and 13 are effectively positively sensitive while buses 8, 10, 11 and 12 are effectively negatively sensitive to increase in DFIG-WECS penetration at bus 14. This practically
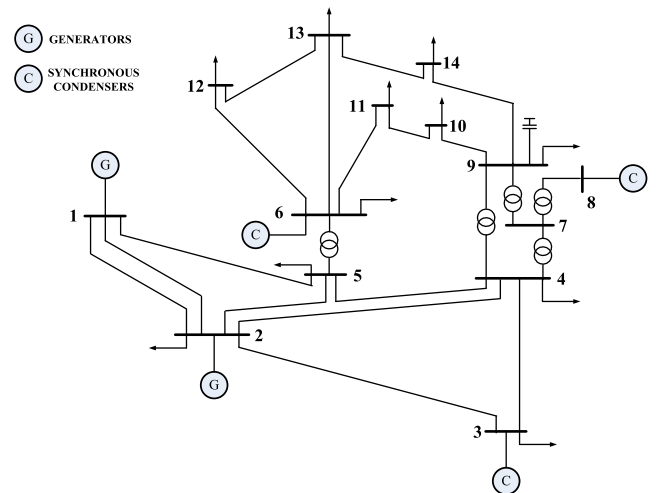
FIGURE 3. IEEE 14-bus network diagram.
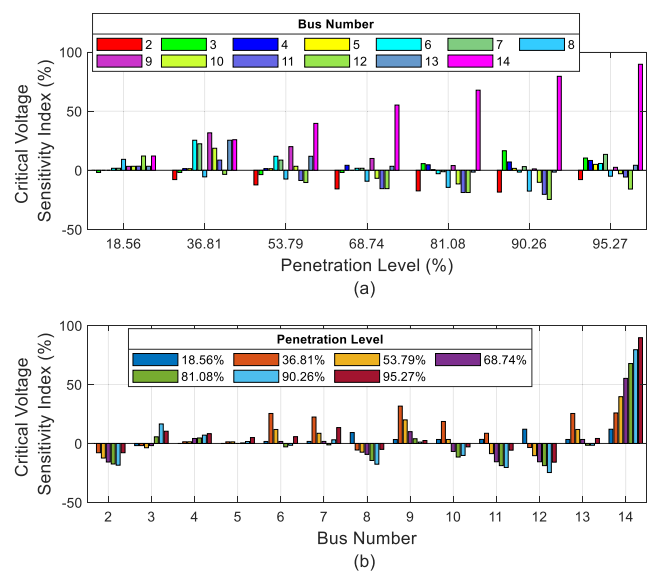
FIGURE 4. CVSI of non-slack buses at different penetration level for case 1.

implies that with increase in DFIG-WECS, bus 14 has the highest rise in critical voltage as the PL increases. On the other hand, bus 2 is the most negatively sensitive bus, which indicates that the critical voltage level at the bus continues to drop as the PL increases.

The corresponding bar chart for the critical reactive power sensitivity index is shown in Fig. 5a and 5b. The practical significance of Q_{CSI} is that it measures the intolerance of a bus to loss of reactive power as the RE penetration level increases. The more positive (negative) the Q_{CSI} value for a bus at a particular PL, the more (less) intolerant the bus is to loss of reactive power at that bus. It can be observed from Fig. 5b that the Q_{CSI} for bus 2 becomes more positive as the DFIG-WECS PL increases. However, the reactive power loss intolerance of all the other buses reduces at first, and then eventually increases at higher penetration levels. In particular, bus 14 becomes significantly intolerant to loss of reactive
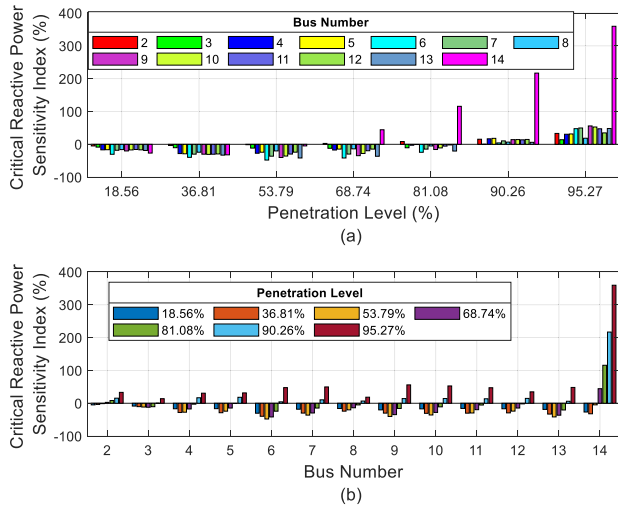
FIGURE 5. CQSI of non-slack buses at different penetration level for case 1.
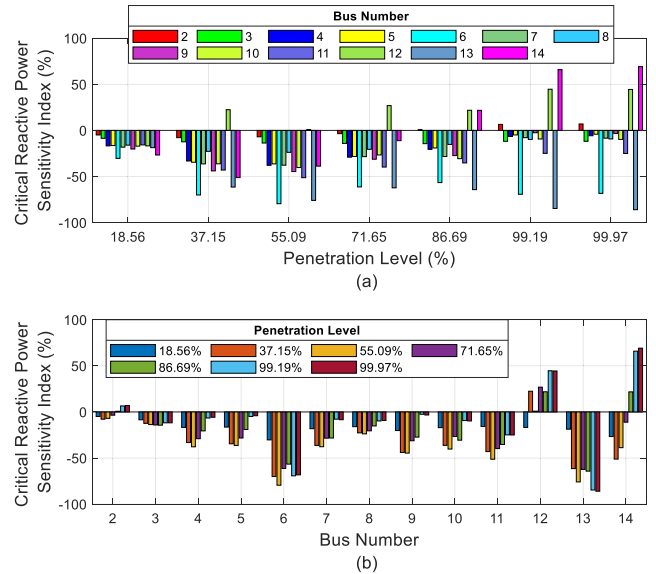

FIGURE 6. CVSI of non-slack buses at different penetration level for Case 2.
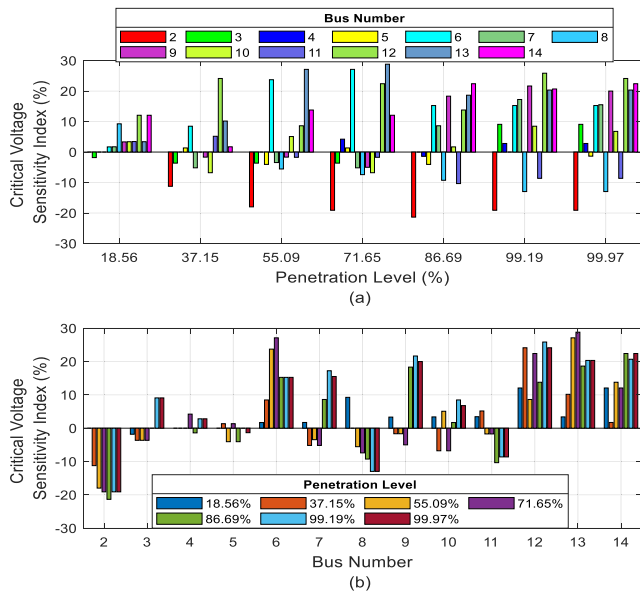

FIGURE 7. CQSI of non-slack buses at different penetration level for case 2.

power at 68.74% and above. At 81.06% PL, the Q_{CSI} of bus 14 is greater than 100%, which indicates that voltage collapse has occurred.

B. CASE 2: DFIG-BASED WECS LOCATED AT BUS 14 AND SOLAR PV LOCATED AT BUS 12

In this case, we consider the integration of DFIG-based WECS and PV system located at bus 14 and bus 12 respectively. In this case, the RE PL is increased from 0MW (0%) PL to 303.23MW (99.97%) PL. The MW value of the maximum PL is as determined by the load flow.

Fig. 6 shows the bar chart of the CVSI for all the buses at the specified PL. Fig. 6a shows the V_{CSI} plot with respect to the percentage PL while Fig. 6b depicts V_{CSI} with respect

to the bus numbers. The charts indicate that bus 2 is negatively sensitive at all penetration levels in regard to critical voltage level. Buses 6, 12, 13, and 14 are positively sensitive at all penetration levels, with bus 12 having the overall highest positive V_{CSI} value. Buses 3, 4, 7, 9 and 10 are effectively positively sensitive while buses 5, 8, and 11 are effectively negatively sensitive to increase in DFIG-WECS and PV system penetration. This shows that with increase in DFIG-WECS at bus 14 and PV system at bus 12, bus 12 has the highest cumulative rise in critical voltage level as the RE PL increases. On the other hand, bus 2 is the most negatively sensitive bus, which indicates that it has the highest fall in critical voltage level as the PL increases.

Fig. 7 shows the corresponding bar chart for the CQSI of the buses at the specified PL. As observed from the figure, buses 6 and 13 have significantly negative Q_{CSI} at all specified PLs, and this implies that the two buses are most tolerant to loss of reactive power. Buses 12 and 14 have the highest reactive power loss intolerance as indicated by their Q_{CSI} values. However, unlike in Case 1, Q_{CSI} of all buses is less than 100% at all PL. This shows that the system does not experience voltage collapse at any PL of the combined DFIG-WECS and PV system.

C. CASE 3: ONLY DFIG-BASED WECS LOCATED AT BUS 2

This section presents the analysis of the third case when DFIG-WECS is located at bus 2, which is the strongest bus within the system. In this case, the RE PL is increased from 0MW (0%) PL to 270MW (99.86%) PL. The MW value of this maximum PL is as determined by the load flow. The following DFIG-WECS PL has been considered:

- No RE integration ≡ 0% PL
- 50MW DFIG-WECS ≡ 18.36% PL
- 100MW DFIG-WECS ≡ 36.98% PL
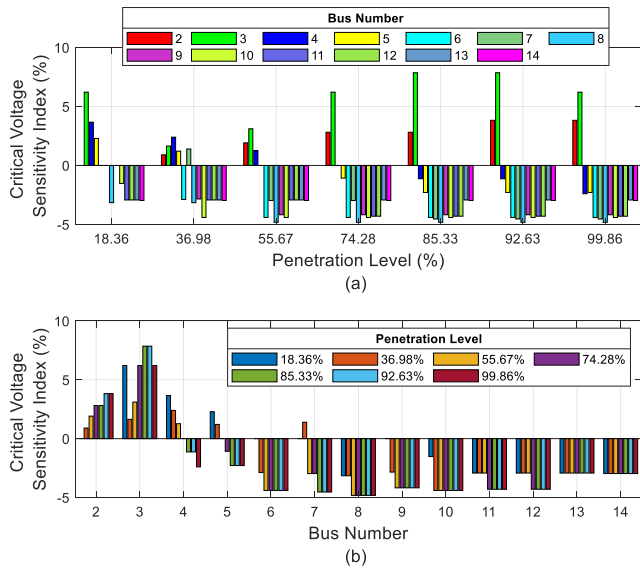
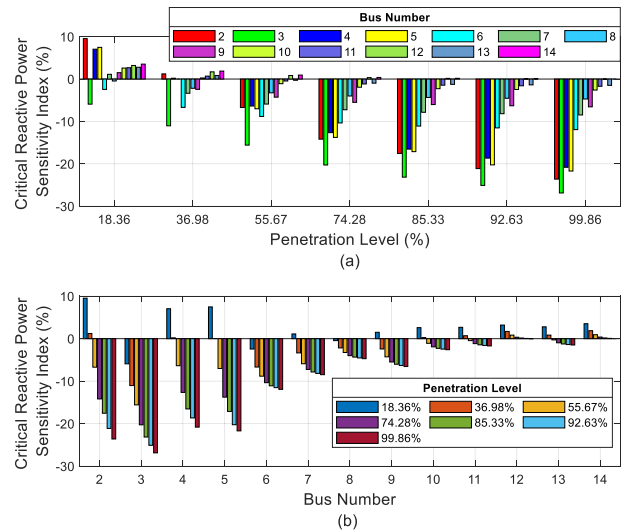**FIGURE 8.** CVSI of non-slack buses at different penetration level for case 3.

- 150MW DFIG-WECS ≡ 55.67% PL
- 200MW DFIG-WECS ≡ 74.28% PL
- 230MW DFIG-WECS ≡ 85.33% PL
- 250MW DFIG-WECS ≡ 92.63% PL
- 270MW DFIG-WECS ≡ 99.86% PL

Fig. 8 shows the bar chart of the CVSI for all the buses at the specified PL. Fig. 8a shows the V_{CSI} plot with respect to the percentage PL while Fig. 8b depicts V_{CSI} with respect to the bus numbers. In this case, bus 3 has the highest rise in critical voltage with increasing DFIG-WECS PL followed by bus 2, which is the point of penetration and then bus 4. All other buses are effectively negatively sensitive to increase in DFIG-WECS PL at bus 2. This indicates that their critical voltage levels fall with increasing PL and bus 8 has the highest cumulative fall in critical voltage.

Fig. 9 shows the corresponding bar chart for the CQSI of the buses at the specified PL. Although buses 3 and 2 have the highest rise in critical voltage, however, their CQSI values depicted in Fig. 9 indicate that they are most tolerant to loss of reactive power. On the other hand, the figure shows that buses 14 and 12 have the highest cumulative positive Q_{CSI}, which indicates that they are most intolerant to loss of reactive power. For this case, the power system does not experience voltage collapse at any DFIG-WECS PL since the Q_{CSI} of all buses is less than 100% at all PL.

D. CASE 4: DFIG-BASED WECS LOCATED AT BUS 2 AND SOLAR PV LOCATED AT BUS 5

This section presents the analysis of the fourth case when DFIG-WECS is located at bus 2 and PV system at bus 5, which are the strongest buses within the system. In this case, the RE PL is increased from 0MW (0%) PL to 265.61MW (100%) PL. The MW value of this maximum PL is as determined by the load flow.

FIGURE 9. CQSI of non-slack buses at different penetration level for case 3.
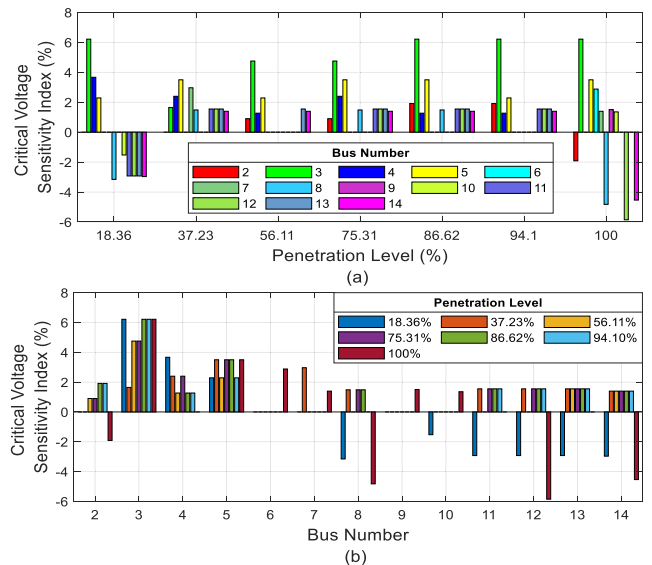
FIGURE 10. CVSI of non-slack buses at different penetration level for case 4.

Fig. 10 shows the bar chart of the CVSI for all the buses at the specified PL. Fig. 10a shows the V_{CSI} plot with respect to the percentage PL while Fig. 10b depicts V_{CSI} with respect to the bus numbers. In this case also, bus 3 has the highest rise in critical voltage as the RE penetration increases followed by bus 5, which is the point of PV system penetration and then bus 4. Buses 6, 7, 9 and 10 are critical voltage-invariant at most of the specified PLs. In general, the CVSI of the buses in this case are relatively insignificant compared to cases 1, 2 and 3. The highest rise in critical voltage in this case is 6.22% recorded for bus 3 at 18.26%, 86.62%, 94.10%, and 100% penetration levels, while the highest fall in critical voltage is −5.85% recorded for bus 12 at 100% PL. These show that the critical voltage levels of the buses are relatively more stable than in the first three cases.
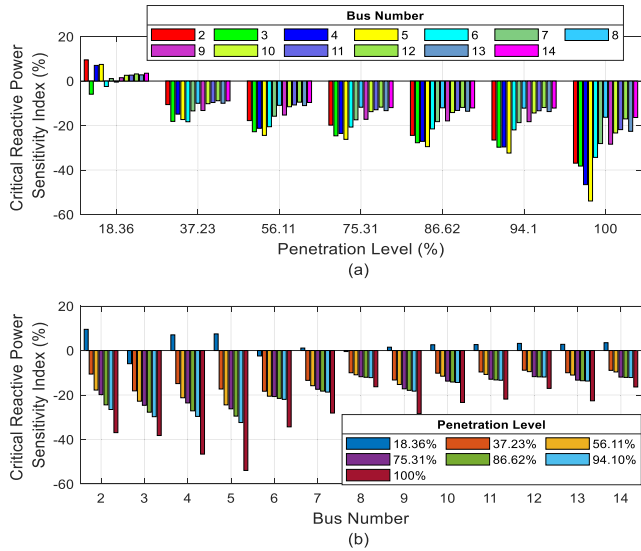
FIGURE 11. CQSI of non-slack buses at different penetration level for case 4.

Fig. 11 shows the corresponding bar chart for the CQSI of the non-slack buses at the specified PL. In this case, the figure reveals that the CQSI values of all buses are negative from 37.23% PL onward. This shows that all the buses become increasingly tolerant to loss of reactive power as the renewable energy PL increases. As observed from the figure, buses 5, 4, 3 and 2 are most tolerant to loss of reactive power as indicated by their CQSI values. Thus, these buses can accommodate larger reactive loads compared to other buses. It can also be noted that in this case the power system is far from experiencing voltage collapse at any PL since the Q_{CSI} of all buses is significantly less than 100% at all PL.

V. IEEE 39-BUS NEW ENGLAND SYSTEM CASE STUDY

In this section, IEEE 39-bus New England Test System is the case study system. IEEE 39-bus New England Test System comprises 10 generators, 19 loads, 12 tie-line buses (interconnecting buses), 34 transmission lines and 12 transformers. The single line diagram of the system is shown in Fig. 12. Detailed data of the system are specified in [47]. In this case, the conventional generator sources are replaced with DFIG-based WECS and PV system in succession.

Fig. 13 shows the bar chart of the CVSI for all the non-slack buses at the specified PL. Buses 1, 2, 9, 18 and 25 have the highest cumulative rise in critical voltage as the PL increases. However, the critical voltage levels of buses 28 and 29 are least affected by increase in RE penetration level.

The corresponding bar chart of the CQSI for the non-slack buses of the IEEE 39-bus system at the specified PL is depicted in Fig. 14. The figure shows that the CQSI values of all the buses are below 100% until at 89.27% PL when the CQSI of bus 32 increased to about 118%. This indicates that the system experiences voltage collapse at 89.27% and bus 32 is the most intolerant bus to loss of reactive power followed by buses 34 and 33. It can also be observed from
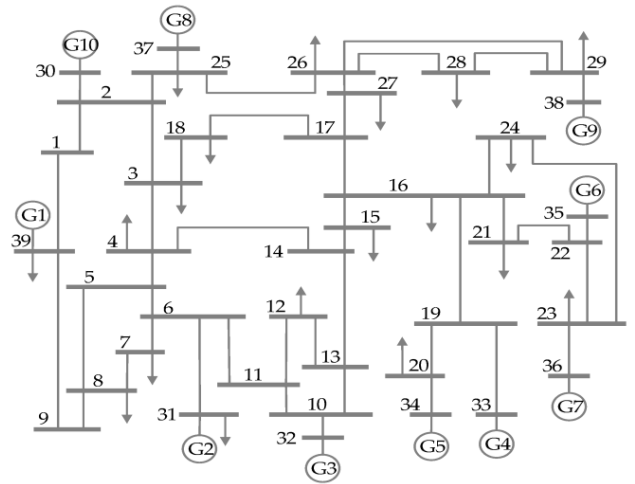

FIGURE 12. Single-line diagram of IEEE 39-bus New England test system [48].
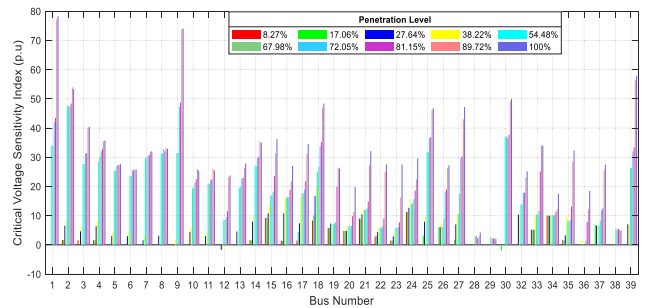

FIGURE 13. CVSI of non-slack buses at different penetration level for IEEE 39-bus New England system.
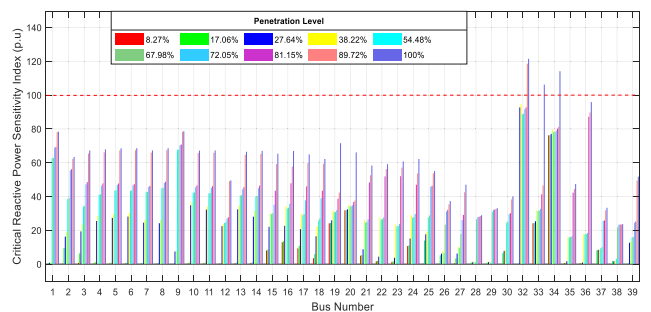
FIGURE 14. CQSI of non-slack buses at different penetration level for IEEE 39-bus New England system.

the figure that the CQSI values of all buses becomes more positive as the PL increases. This indicates that all the buses become increasingly intolerant to loss of reactive power as the renewable energy PL increases.

VI. CONCLUSION

A QV-based approach to determine the voltage instability sensitivities of power system buses to increase in renewable energy penetration level has been developed and discussed in this paper. This paper can be summarised as follows:

- Two sensitivity indices, namely, Critical Voltage Sensitivity Index (CVSI) and Critical Reactive Power Sensitivity Index (CQSI) have been developed and utilised to assess the voltage instability sensitivities of power system buses when there is increasing penetration level of DFIG-WECS+PV system. The CVSI measures the impact of increasing RE PL on the rise in critical voltage level of each bus in the system and the CQSI evaluates the impact of increasing RE PL on the intolerance of each bus to loss of reactive power.

- The proposed indices have been tested on IEEE 14-bus system and IEEE 39-bus New England Test System. The results of the analyses on the IEEE 14-bus system for the four cases indicate that when DFIG-based WECS and PV system are located on weak buses, the reactive power loss intolerance of the power system buses are higher than when they are located at the strongest buses. Also, with increasing DFIG-based WECS alone at the weakest bus 14, the voltage stability of the system is initially enhanced but later declines at higher PLs. Bus 14 becomes significantly intolerant to loss of reactive power at 68.74% and consequently, voltage collapse occurs at 81.06% PL, when its Q_{CSI} becomes greater than 100%. However, the results shows that when PV system is introduced in Case 2, the voltage stability of the system is effectively enhanced compared to the case of DFIG-based WECS only.

- The bus sensitivity analysis carried out in this work is not limited to load buses only. All buses except the slack bus have been analysed. This gives a better evaluation of the system's sensitivity to increase in RE PL. As observed in the case of the IEEE 39-bus New England System, all the buses become increasingly intolerant to loss of reactive power as the RE PL increases. However, the buses which are most affected by increase in RE PL are generator buses. In particular, the CQSI of generator bus 32 exceeds 100% at 89.27% PL, indicating that voltage collapse has occurred. Thus, the sensitivity indices proposed in this work gives a more comprehensive overview of the power system's voltage instability sensitivity with increase in RE PL.

- The voltage instability sensitivities of power system buses carried out in this work can provide insights on the most optimal placement for large reactive loads and reactive power compensation devices as the RE PL increases, since they have significant influence on the reactive power capability of the system when they absorb/inject reactive power into the power system. Appropriate FACTS devices can be located in the bus which is most prone to voltage instability, in order to improve the stability of the system.

- The subject of system reconfiguration as a means of reducing instability and the associated cost can be investigated in future studies.

REFERENCES

[1] T. R. Ayodele, A. S. O. Ogunjuyigbe, and B. B. Adetokun, "Optimal capacitance selection for a wind-driven self-excited reluctance generator under varying wind speed and load conditions," *Appl. Energy*, vol. 190, pp. 339–353, Mar. 2017.

[2] S. Jerez, I. Tobin, M. Turco, P. Jiménez-Guerrero, R. Vautard, and J. P. Montávez, "Future changes, or lack thereof, in the temporal variability of the combined wind-plus-solar power production in Europe," *Renew. Energy*, vol. 139, pp. 251–260, Aug. 2019.

[3] B. P. Heard, B. W. Brook, T. M. L. Wigley, and C. J. A. Bradshaw, "Burden of proof: A comprehensive review of the feasibility of 100% renewable-electricity systems," *Renew. Sustain. Energy Rev.*, vol. 76, pp. 1122–1133, Sep. 2017.

[4] T. W. Brown, T. Bischof-Niemz, K. Blok, C. Breyer, H. Lund, and B. V. Mathiesen, "Response to 'Burden of proof: A comprehensive review of the feasibility of 100% renewable-electricity systems,'" *Renew. Sustain. Energy Rev.*, vol. 92, pp. 834–847, Jan. 2018.

[5] M. Child, C. Kemfert, D. Bogdanov, and C. Breyer, "Flexible electricity generation, grid exchange and storage for the transition to a 100% renewable energy system in Europe," *Renew. Energy*, vol. 139, pp. 80–101, Aug. 2019.

[6] B. Kroposki, B. Johnson, Y. Zhang, V. Gevorgian, P. Denholm, B.-M. Hodge, and B. Hannegan, "Achieving a 100% renewable grid: Operating electric power systems with extremely high levels of variable renewable energy," *IEEE Power Energy Mag.*, vol. 15, no. 2, pp. 61–73, Mar. 2017.

[7] S. D. Ahmed, F. S. M. Al-Ismail, M. Shafiullah, F. A. Al-Sulaiman, and I. M. El-Amin, "Grid integration challenges of wind energy: A review," *IEEE Access*, vol. 8, pp. 10857–10878, 2020.

[8] M. N. I. Sarkar, L. G. Meegahapola, and M. Datta, "Reactive power management in renewable rich power grids: A review of grid-codes, renewable generators, support devices, control strategies and optimization algorithms," *IEEE Access*, vol. 6, pp. 41458–41489, 2018.

[9] Z. Tang, D. J. Hill, and T. Liu, "Two-stage voltage control of subtransmission networks with high penetration of wind power," *Control Eng. Pract.*, vol. 62, pp. 1–10, May 2017.

[10] B. B. Adetokun, C. M. Muriithi, and J. O. Ojo, "Voltage stability assessment and enhancement of power grid with increasing wind energy penetration," *Int. J. Electr. Power Energy Syst.*, vol. 120, Sep. 2020, Art. no. 105988.

[11] I. G. Adebayo and Y. Sun, "Voltage stability based on a novel critical bus identification index," in *Proc. 14th IEEE Conf. Ind. Electron. Appl. (ICIEA)*, Jun. 2019, pp. 1777–1782.

[12] Y. Zheng, D. J. Hill, K. Meng, and S. Y. Hui, "Critical bus voltage support in distribution systems with electric springs and responsibility sharing," *IEEE Trans. Power Syst.*, vol. 32, no. 5, pp. 3584–3593, Sep. 2017.

[13] M. M. Salama, E. M. Saied, M. M. Abou-Elsaad, and E. F. Ghariany, "Estimating the voltage collapse proximity indicator using artificial neural network," *Energy Convers. Manage.*, vol. 42, no. 1, pp. 69–79, Jan. 2001.

[14] H. Chen, T. Jiang, H. Yuan, H. Jia, L. Bai, and F. Li, "Wide-area measurement-based voltage stability sensitivity and its application in voltage control," *Int. J. Electr. Power Energy Syst.*, vol. 88, pp. 87–98, Jun. 2017.

[15] S. Pérez-Londoño, L. F. Rodríguez, and G. Olivar, "A simplified voltage stability index (SVSI)," *Int. J. Electr. Power Energy Syst.*, vol. 63, pp. 806–813, Dec. 2014.

[16] N. V. Acharya and P. S. N. Rao, "A new voltage stability index based on the tangent vector of the power flow jacobian," in *Proc. IEEE Innov. Smart Grid Technol.-Asia (ISGT Asia)*, Nov. 2013, pp. 1–6.

[17] L. D. Arya, S. C. Choube, and M. Shrivastava, "Technique for voltage stability assessment using newly developed line voltage stability index," *Energy Convers. Manage.*, vol. 49, no. 2, pp. 267–275, Feb. 2008.

[18] A. Oukennou and A. Sandali, "Assessment and analysis of voltage stability indices in electrical network using PSAT software," in *Proc. 18th Int. Middle East Power Syst. Conf. (MEPCON)*, Dec. 2016, pp. 705–710.

[19] S. Ratra, R. Tiwari, and K. R. Niazi, "Voltage stability assessment in power systems using line voltage stability index," *Comput. Electr. Eng.*, vol. 70, pp. 199–211, Aug. 2018.

[20] A. Rabiee, M. Vanouni, and M. Parniani, "Optimal reactive power dispatch for improving voltage stability margin using a local voltage stability index," *Energy Convers. Manage.*, vol. 59, pp. 66–73, Jul. 2012.

[21] M. H. Haque, "Use of local information to determine the distance to voltage collapse," in *Proc. Int. Power Eng. Conf. (IPEC)*, 2007, pp. 407–412.

[22] V. Balamourougan, T. S. Sidhu, and M. S. Sachdev, "Technique for online prediction of voltage collapse," *IEE Proc.-Gener., Transmiss. Distrib.*, vol. 151, no. 4, pp. 453–460, 2004.

[23] M. S. S. Danish, T. Senjyu, S. M. S. Danish, N. R. Sabory, and N. K. P. Mandal, "A recap of voltage stability indices in the past three decades," *Energies*, vol. 12, no. 8, p. 1544, Apr. 2019.

[24] J. Modarresi, E. Gholipour, and A. Khodabakhshian, "A comprehensive review of the voltage stability indices," *Renew. Sustain. Energy Rev.*, vol. 63, pp. 1–12, Sep. 2016.

[25] O. B. Adewuyi, R. Shigenobu, T. Senjyu, M. E. Lotfy, and A. M. Howlader, "Multiobjective mix generation planning considering utility-scale solar PV system and voltage stability: Nigerian case study," *Electric Power Syst. Res.*, vol. 168, pp. 269–282, Mar. 2019.

[26] L. Gan, G. Li, and M. Zhou, "Coordinated planning of large-scale wind farm integration system and regional transmission network considering static voltage stability constraints," *Electr. Power Syst. Res.*, vol. 136, pp. 298–308, Jul. 2016.

[27] X. Bian, Y. Geng, F. Yuan, K. L. Lo, and Y. Fu, "Identification and improvement of probabilistic voltage instability modes of power system with wind power integration," *Electr. Power Syst. Res.*, vol. 140, pp. 162–172, Nov. 2016.

[28] L. Chen, Y. Min, Y. Dai, and M. Wang, "Stability mechanism and emergency control of power system with wind power integration," *IET Renew. Power Gener.*, vol. 11, no. 1, pp. 3–9, Jan. 2017.

[29] X. Liu, G. Wu, and X. Li, "Study on voltage stability and control strategy of grid-connected wind farm," *IEEE Access*, vol. 7, pp. 148843–148852, 2019.

[30] J. N. da Costa, J. A. P. Filho, and R. M. Henriques, "Loading margin sensitivity analysis in systems with significant wind power generation penetration," *Electr. Power Syst. Res.*, vol. 175, Oct. 2019, Art. no. 105900.

[31] A. Mitra and D. Chatterjee, "A sensitivity based approach to assess the impacts of integration of variable speed wind farms on the transient stability of power systems," *Renew. Energy*, vol. 60, pp. 662–671, Dec. 2013.

[32] H. Zhou, S. Chen, J. Lai, X. Lu, C. Yu, W. Hu, Q. Deng, and D. Zhou, "Modeling and synchronization stability of low-voltage active distribution networks with large-scale distributed generations," *IEEE Access*, vol. 6, pp. 70989–71002, 2018.

[33] S. S. Refaat, H. Abu-Rub, A. P. Sanfilippo, and A. Mohamed, "Impact of grid-tied large-scale photovoltaic system on dynamic voltage stability of electric power grids," *IET Renew. Power Gener.*, vol. 12, no. 2, pp. 157–164, Feb. 2018.

[34] D. Q. Hung, N. Mithulananthan, and R. C. Bansal, "Integration of PV and BES units in commercial distribution systems considering energy loss and voltage stability," *Appl. Energy*, vol. 113, pp. 1162–1170, Jan. 2014.

[35] W. Jin and Y. Lu, "Stability analysis and oscillation mechanism of the DFIG-based wind power system," *IEEE Access*, vol. 7, pp. 88937–88948, 2019.

[36] M. Yu, A. J. Roscoe, C. D. Booth, A. Dysko, R. Ierna, J. Zhu, N. Grid, and H. Urdal, "Use of an inertia-less virtual synchronous machine within future power networks with high penetrations of converters," in *Proc. Power Syst. Comput. Conf. (PSCC)*, Jun. 2016, pp. 1–7.

[37] O. P. Mahela, N. Gupta, M. Khosravy, and N. Patel, "Comprehensive overview of low voltage ride through methods of grid integrated wind generator," *IEEE Access*, vol. 7, pp. 99299–99326, 2019.

[38] A. S. O. Ogunjuyigbe, T. R. Ayodele, and B. B. Adetokun, "Steady state analysis of wind-driven self-excited reluctance generator for isolated applications," *Renew. Energy*, vol. 114, pp. 984–1004, Dec. 2017.

[39] A. Benali, M. Khiat, T. Allaoui, and M. Denai, "Power quality improvement and low voltage ride through capability in hybrid wind-PV farms grid-connected using dynamic voltage restorer," *IEEE Access*, vol. 6, pp. 68634–68648, 2018.

[40] K. Z. Heetun, S. H. E. Abdel Aleem, and A. F. Zobaa, "Voltage stability analysis of grid-connected wind farms with FACTS: Static and dynamic analysis," *Energy Policy Res.*, vol. 3, no. 1, pp. 1–12, Jan. 2016.

[41] Y. Lei, A. Mullane, G. Lightbody, and R. Yacamini, "Modeling of the wind turbine with a doubly fed induction generator for grid integration studies," *IEEE Trans. Energy Convers.*, vol. 21, no. 1, pp. 257–264, Mar. 2006.

[42] B. Yang, X. Zhang, T. Yu, H. Shu, and Z. Fang, "Grouped grey wolf optimizer for maximum power point tracking of doubly-fed induction generator based wind turbine," *Energy Convers. Manage.*, vol. 133, pp. 427–443, Feb. 2017.

[43] M. G. Molina, "Modelling and control of grid-connected solar photovoltaic systems," in *Renewable Energy: Utilisation and System Integration*, W. Cao and Y. Hu, Eds. Rijeka, Croatia: InTech, 2016, pp. 53–83.

[44] C. Reis and F. P. M. Barbosa, "A comparison of voltage stability indices," in *Proc. IEEE Medit. Electrotech.Conf. (MELECON)*, 2006, pp. 1007–1010.

[45] J. S. Bhonsle, S. B. Deshpande, M. M. Renge, and R. V. Harne, "A new approach for determining weakest bus and voltage stability margin in a power system," in *Proc. Nat. Power Syst. Conf.*, 2004, pp. 102–107.

[46] DIgSILENT PowerFactory, "14 bus System," *DIgSILENT GmbH*, pp. 1–8, 2019.

[47] DIgSILENT PowerFactory, "39 bus New England system," *DIgSILENT GmbH*, pp. 1–15, 2019.

[48] C. Jin, W. Li, L. Liu, P. Li, and X. Wu, "A coherency identification method of active frequency response control based on support vector clustering for bulk power system," *Energies*, vol. 12, no. 16, p. 3155, 2019.

BUKOLA BABATUNDE ADETOKUN (Graduate Student Member, IEEE) was born in Ibadan, Nigeria. He received the B.Sc. and M.Sc. degrees in electrical and electronic engineering from the University of Ibadan, in 2012 and 2016, respectively.

He was a Research Assistant at the Power, Energy, Machines and Drives Research Group, Department of Electrical and Electronic Engineering, University of Ibadan, from 2014 to 2016 and a Lecturer II at Covenant University, Ota, Nigeria, in 2017. He is currently a Ph.D. Scholar at the Pan African University Institute for Basic Sciences, Technology and Innovation, hosted at Jomo Kenyatta University of Technology and Agriculture, Kenya. His current research interests include renewable energy conversion systems and grid integration, power system stability, and application of FACTS devices.

JOSEPH OLORUNFEMI OJO (Fellow, IEEE) was born in Kabba, Nigeria. He received the bachelor's and master's degrees in electrical engineering from Ahmadu Bello University, Zaria, Nigeria, and the Ph.D. degree from the University of Wisconsin–Madison, Madison, WI, USA.

He is currently a Professor of electrical and computer engineering at Tennessee Technological University, Cookeville, TN, USA. His current research interests span the areas of electric machine analysis and drive control, switching converter technology and modern control applications in converter-enhanced power, and distributed energy generation systems.

Dr. Ojo is a Fellow of the Institute of Electrical Engineers (FIEE). He was the Chair of the Industrial Power Converter System Department of the IEEE Industry Application Society. He is also an Associate Editor of the IEEE Transactions on Power Electronics. He is currently the Editor-in-Chief of the IEEE Journal of Emerging and Selected Topics in Power Electronics.

CHRISTOPHER MAINA MURIITHI (Member, IEEE) received the B.Sc. and M.Sc. degrees in electrical power engineering from the Moscow Power Engineering Institute, National University, in 2001 and 2003, respectively, and the Ph.D. degree in electrical engineering from the Jomo Kenyatta University of Agriculture and Technology.

He is currently an Associate Professor of electrical engineering and the Dean of the School of Engineering and Technology, Murang'a University of Technology. His research interests include power systems analysis, artificial intelligence applications, and renewable energy technologies.

• • •